

FINO: Flow-based Joint Image and Noise Model

Lanqing Guo¹, Siyu Huang¹, Haosen Liu² and Bihan Wen¹

¹School of Electrical & Electronic Engineering, Nanyang Technological University, Singapore

²SmartMore Corporation, China

{lanqing001, siyu.huang, bihan.wen}@ntu.edu.sg

haosen.liu0803@gmail.com

Abstract

One of the fundamental challenges in image restoration is denoising, where the objective is to estimate the clean image from its noisy measurements. To tackle such an ill-posed inverse problem, the existing denoising approaches generally focus on exploiting effective natural image priors. The utilization and analysis of the noise model are often ignored, although the noise model can provide complementary information to the denoising algorithms. In this paper, we propose a novel Flow-based joint Image and NOise model (FINO) that distinctly decouples the image and noise in the latent space and losslessly reconstructs them via a series of invertible transformations. We further present a variable swapping strategy to align structural information in images and a noise correlation matrix to constrain the noise based on spatially minimized correlation information. Experimental results demonstrate FINO’s capacity to remove both synthetic additive white Gaussian noise (AWGN) and real noise. Furthermore, the generalization of FINO to the removal of spatially variant noise and noise with inaccurate estimation surpasses that of the popular and state-of-the-art methods by large margins.

Introduction

Image denoising refers to recovering the underlying clean image from an observed noisy measurement. Despite today’s vast improvement in camera sensors, digital images are often corrupted by severe noises in complex environments, resulting in nontrivial effects to subsequent vision tasks.

Existing image denoising methods generally rely on the construction of effective image priors. For conventional methods, the corresponding priors include, *e.g.*, sparsity (Elad and Aharon 2006; Ravishankar and Bresler 2012) and low-rankness (Gu et al. 2014). By shrinkage or filtering in the transform domain, image components that are satisfied with the prior are preserved in the denoised results. However, these priors are usually applied to image patches, lacking patch consensus and global modeling. Recently, the deep learning approaches (Zhang et al. 2017; Zhang, Zuo, and Zhang 2018; Liu et al. 2018) have achieved state-of-the-art image denoising results by relying on an external training

Copyright © 2022, Association for the Advancement of Artificial Intelligence (www.aaai.org). All rights reserved.

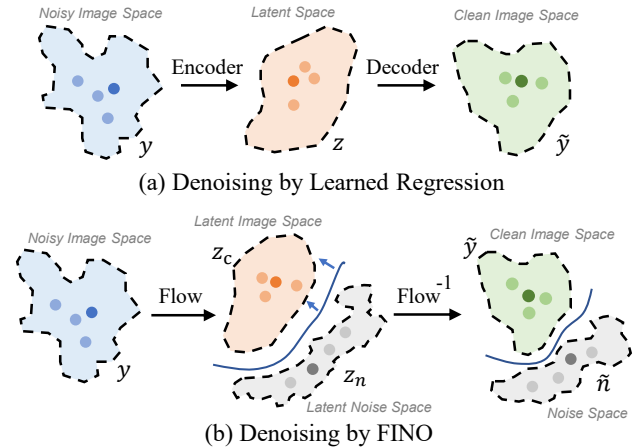


Figure 1: The framework of Flow-based Joint Image and Noise Model (FINO) and comparison between previous regression-based denoisers (a) and the proposed FINO (b).

corpus. These deep denoisers generally learn a direct mapping from noisy images to clean images, where the learned models serve as an effective prior on the clean image space. Despite the success of learning effective image priors for denoising, few work to-date investigated the noise modeling that is complementary to the deep image priors learning. In practice, the residual between the noisy image and the denoised one always contains image structures that are wrongly removed together with noise. These structures generally correspond to high-frequency components of an image, which are distinct from the random noise. This inspires us that it might be possible to constrain the residual map with the noise model to ‘squeezing’ image information from the residual map.

Different from all existing deep denoising methods, we reformulate the image denoising task as a dual modeling problem of both the image and noise (as illustrated in Figure 1(b)), instead of only reconstructing the noise-free image (Figure 1(a)). However, *how to achieve an effective decoupling of clean image and noise* is still a challenging and under-explored problem in the existing literature. In this paper, we show that the noisy images can be losslessly transformed to a more distinguishable feature space through a

novelly proposed framework named **Flow-based joint Image and NOise model (FINO)**. FINO losslessly decouples the image-noise components in the latent space through a forward process of the flow-based invertible network. Then, the decoupled components can be reconstructed as the noise and image in the spatial domain through a backward process of an invertible network. Based on the decoupled noise and image components, we further introduce a noise variable swapping strategy to align the structural information in images, as well as a constraint on the noise correlation matrix to be spatially independent on the neighboring regions. Extensive experiments are conducted to evaluate FINO on both the synthetic noise and real noise removal tasks. Empirical results show that FINO achieves superior performances in comparison with the state-of-the-art image denoising methods. Besides, FINO provides significantly better generalizability than the existing denoising methods.

The contributions of this work are summarized as follow:

- We propose to jointly model the distributions of the image and noise for denoising tasks, showing that the noise model can provide abundant and complementary information, in addition to image priors.
- We present a novel image denoising framework named FINO which distinctly disentangles the noise and the noise-free image in the latent space. Two learning methods, including variable swapping and noise correlation matrix, are also proposed to improve the learning of FINO.
- We conduct extensive experiments on both the synthetic and real noise datasets. FINO shows superior denoising and generalization performances compared to the existing denoising methods.

Related Work

Image Denoising

Model-based image denoising. Image denoising is a typical ill-posed problem with the goal of recovering high-quality images from their noisy measurements. Numerous efforts have been made towards it over the past decades. Classic methods generally take advantage of the image priors, such as sparsity (Elad and Aharon 2006; Ravishankar and Bresler 2012), low rank (Gu et al. 2014), and non-local self-similarity (Dabov et al. 2007; Xu et al. 2015), to address the denoising problem. Most classic denoisers utilize the image features in certain transform domains by applying shrinkages or filtering to the exploitation of image priors. The learning-based transform methods are more flexible, but they all worked on patches, lacking global modeling. Motivated by this, in this work, we employ a flow-based invertible network to conduct a learnable global transforming.

Deep learning based image denoising. In recent years, deep learning-based denoisers exhibit superiority in learning the end-to-end mapping from noisy to clean images (Liu et al. 2018). For instance, Zhang *et al.* (Zhang et al. 2017) achieves a very competitive denoising performance through residual neural networks. Zhang *et al.* (Zhang, Zuo, and Zhang 2018) further introduces a noise level map to control

the trade-off between noise reduction and detail preservation. More recently, some researchers (Plötz and Roth 2018; Liu et al. 2018) try to leverage deeper and larger neural networks to achieve better performance. Generally, existing denoising methods focus on exploiting effective natural image priors, while the modeling, analysis, and utilization of the noise component are often ignored. This work jointly models the natural image and noise via invertible neural networks to deliver better denoising performance and visual quality.

More recently, there are some attempts (Yue et al. 2019; Anwar and Barnes 2019; Guo et al. 2019) for denoising on real-noisy images. The attempts can be generally divided into two categories: 1) Two-step denoising (Yue et al. 2019), which first estimates the noise map then reconstructs the clean image non-blindly based on the estimated noise map. 2) One-step denoising with an end-to-end framework (Anwar and Barnes 2019). This work focuses on both real noise and synthetic noise removal. It follows the one-step denoising approaches to enhance the generalization capacity of denoising models.

Neural Flows

The neural flow is a type of deep generative model that learns the exact likelihood of targets through a chain of reversible transformations. The generative process $\mathbf{x} = \mathcal{F}_\theta(\mathbf{z})$ given a latent variable \mathbf{z} can be specified by an invertible architecture \mathcal{F}_θ . The direct access to the inverse mapping is $\mathbf{z} = \mathcal{F}_\theta^{-1}(\mathbf{x})$. As a pioneering work, NICE (Dinh, Krueger, and Bengio 2014) learns a highly non-linear bijective transformation that maps the training data to a space where its distribution is factorized. Following NICE, more effective and flexible transformations have been proposed (Dinh, Sohl-Dickstein, and Bengio 2016; Ho et al. 2019; Kingma and Dhariwal 2018).

More recently, a series of works exploit neural flows for image restoration (Abdelhamed, Brubaker, and Brown 2019; Lugmayr et al. 2020; Xiao et al. 2020; Liu et al. 2021), which formulate image restoration as a non-degradation image generation problem. For instance, SRFlow (Lugmayr et al. 2020) designs a conditional normalizing flow architecture for super-resolution, which learns the distribution of realistic HR images. (Xiao et al. 2020) and (Liu et al. 2021) apply invertible networks to image rescaling and image denoising tasks, respectively. InvDN (Liu et al. 2021) focuses on real noise removal and detours the noise-image disentanglement. It splits noisy images into low-frequency and high-frequency components and then directly drops the high-frequency component, restoring the image based on the low-frequency component only, which may result in information loss and over-smoothness. Different from InvDN, our proposed FINO utilizes an invertible network to decouple the image content and noise components in the latent space and then reconstruct them in the image space, respectively, achieving a lossless image-noise disentanglement.

Preliminary

In this section, we introduce the preliminary knowledge of the multi-scale neural flow (Ardizzone et al. 2019; Xiao et al.

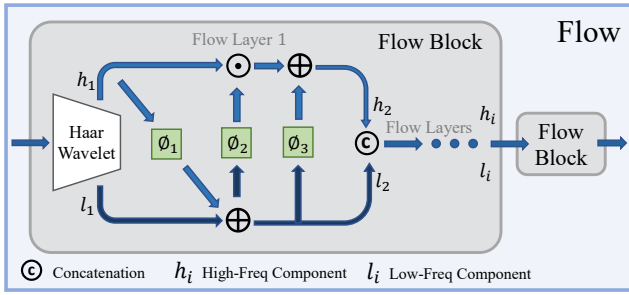


Figure 2: The architecture of neural flow model, consisting of two flow blocks. Each flow block includes an invertible Haar wavelet transformation at first layer and twelve affine coupling layers. i denotes i -th affine coupling layer.

2020; Liu et al. 2021). We denote it as $\text{Flow}(\cdot)$ in this paper. As shown in Figure 2, $\text{Flow}(\cdot)$ consists of a series of flow blocks, and each flow block consists of an invertible wavelet transformation followed by a series of affine coupling layers.

Invertible wavelet transform. To disentangle the information of clean image and noise, we employ invertible Haar wavelet transformation at the first layer of each flow block to downsample the input images/features and to increase the feature channels (Xiao et al. 2020). After the wavelet transformation, the input image/features with a shape of (H, W, C) should be squeezed into $(H/2, W/2, 4C)$. $4C$ denotes three directions of high-frequency coefficients and one low-frequency representation (Kingsbury and Magarey 1998). The invertible wavelet transformation provides the separated low and high-frequency information to the following invertible neural layers.

Affine coupling layers. After the wavelet transformation layer, the input image/feature \mathbf{u}_i has been splitted into low and high-frequency components, denoted as \mathbf{h}_i and \mathbf{l}_i , respectively. We leverage the coupling layer (Dinh, Krueger, and Bengio 2014) to further decouple the structural information and the degradation bias. Suppose the i -th coupling layer’s input is \mathbf{u}_i and the output is \mathbf{u}_{i+1} ($i = 1 \dots I$), the forward procedure in this block is

$$\begin{aligned}
 \mathbf{l}_i, \mathbf{h}_i &= \text{Split}(\mathbf{u}_i), \\
 \mathbf{l}_{i+1} &= \mathbf{l}_i + \phi_1(\mathbf{h}_i), \\
 \mathbf{h}_{i+1} &= \phi_2(\mathbf{l}_{i+1}) \odot \mathbf{h}_i + \phi_3(\mathbf{l}_{i+1}), \\
 \mathbf{u}_{i+1} &= \text{Concat}(\mathbf{l}_{i+1}, \mathbf{h}_{i+1}),
 \end{aligned} \tag{1}$$

where $\text{Split}(\cdot)$ denotes channel-wise splitting and $\text{Concat}(\cdot)$ is the corresponding inverse operation. $\phi_1(\cdot)$, $\phi_2(\cdot)$, and $\phi_3(\cdot)$ can be any neural networks that are not required to be invertible. The backward procedure is easily derived as

$$\begin{aligned}
 \mathbf{l}_{i+1}, \mathbf{h}_{i+1} &= \text{Split}(\mathbf{u}_{i+1}), \\
 \mathbf{h}_i &= (\mathbf{h}_{i+1} - \phi_3(\mathbf{l}_{i+1})) / \phi_2(\mathbf{l}_{i+1}), \\
 \mathbf{l}_i &= (\mathbf{l}_{i+1} - \phi_1(\mathbf{h}_i)) / \phi_1(\mathbf{h}_i), \\
 \mathbf{u}_i &= \text{Concat}(\mathbf{l}_i, \mathbf{h}_i).
 \end{aligned} \tag{2}$$

FINO

In this section, we present a neural flow-based framework named FINO to jointly model the image and noise in context of image denoising. We first formulate the image denoising problem, then discuss why employing the invertible neural networks for image-noise disentanglement, and introduce the architecture details of FINO, including the variable swapping in latent space for disentanglement, the clean image regression for image modeling, and the noise correlation matrix for noise modeling, as well as objective functions.

Problem Formulation

A noisy image \mathbf{y} and its noise-free counterpart \mathbf{x} can be formulated as

$$\mathbf{y} = \mathbf{x} + \mathbf{n}, \tag{3}$$

where \mathbf{n} denotes the random noise. Here, we consider both the synthetic noise and the real noise. The synthetic noise is the *i.i.d* additive white Gaussian noise (AWGN). It follows the normal distribution $\mathcal{N}(0, \sigma^2 \cdot \mathbf{I})$. Typical supervised regression-based denoising methods train the deep neural networks (DNNs) by

$$\min_{\theta} \mathbb{E}_{\mathbf{x}, \mathbf{y}} [\mathcal{L}_{reg}(\mathcal{G}_{\theta}(\mathbf{y}), \mathbf{x})], \tag{4}$$

where $\mathcal{G}_{\theta}(\cdot)$ denotes the regression-based denoiser, which can be regarded as the combination of encoder and decoder $\mathcal{D}_{\theta}(\mathcal{E}_{\theta}(\cdot))$. $\mathcal{L}_{reg}(\cdot, \cdot)$ denotes the loss function, *e.g.*, the ℓ_1 or ℓ_2 loss.

Different from the conventional methods, we novelly propose a dual modeling of both noise and image as

$$\min_{\theta} \mathbb{E}_{\mathbf{x}, \mathbf{y}} [\mathcal{L}_{reg}(\mathcal{G}_{\theta}(\mathbf{y}), \mathbf{x}) + \mathcal{L}_{noise}(\mathcal{H}_{\theta}(\mathbf{y}), \mathbf{n})], \tag{5}$$

where $\mathcal{L}_{noise}(\cdot, \cdot)$ denotes the loss function of the noise modeling, and $\mathcal{H}_{\theta}(\cdot)$ denotes the noise model. The proposed FINO disentangles noise and image in a more distinguishable latent space via an invertible network, on behalf of \mathcal{G}_{θ} and \mathcal{H}_{θ} , by jointly modeling image and noise.

Why Disentangling via Invertible Network?

Although it is known that the representation ability of the invertible network is limited and weaker than some more sophisticated deep neural networks, because of its specially designed structure (Kirichenko, Izmailov, and Wilson 2020), there are three main reasons why we choose the invertible network for image-noise decoupling.

- Firstly, existing regression-based image denoising algorithms cannot achieve lossless image reconstruction of the input image: Once the input noisy image is embedded into latent space, some information may get lost. This problem is especially severe for the non-structural information, *e.g.*, noise. Different from them, the invertible network can losslessly encode the image and noise. This property ensures that recoveries of the image and noise can always complement each other, providing the basis of improving the image denoising performance via a joint image and noise modeling.

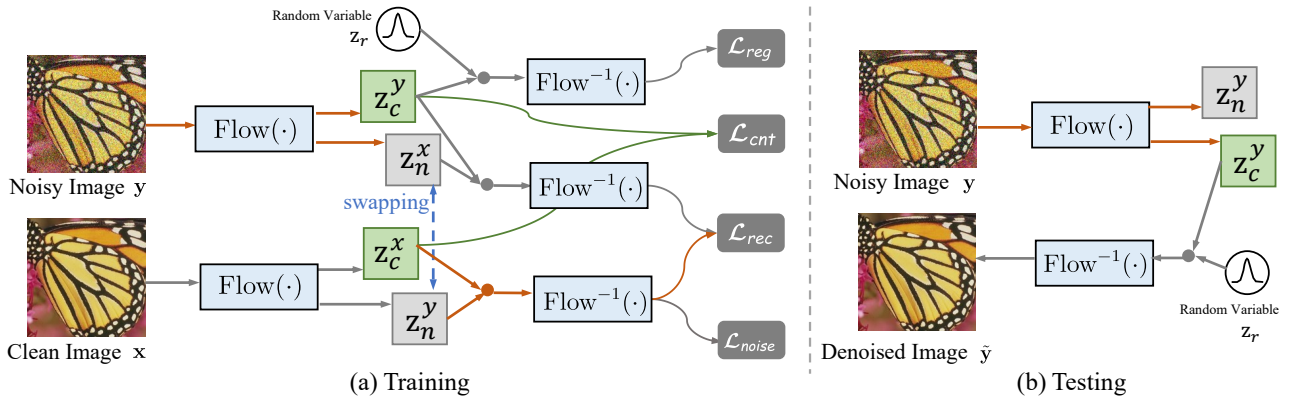


Figure 3: An overview of our Flow-based Joint Image and NOise Model (FINO).

- Secondly, only the forward module of invertible network needs to be trained, while the backward module is the direct inverse, which respectively act as encoder and decoder. The number of free parameters can be thus significantly reduced.
- Finally, image denoising is an ill-posed inverse problem of one-to-many mapping, *i.e.*, one noisy image can be restored to many denoised estimations. Most of the existing methods formulate it as a one-to-one mapping task, *i.e.*, delivering one denoised image from one noisy input. However, FINO can sample diverse denoised images by coupling the disentangled clean image with any random variable sampled from a normal distribution.

The Framework of FINO

Given a noisy image \mathbf{y} and its corresponding clean counterpart \mathbf{x} in training stage, we first employ an invertible flow model $\text{Flow}(\cdot)$ to embed the input pair to latent codes respectively, as

$$\mathbf{z}^x = \text{Flow}(\mathbf{x}) \quad \mathbf{z}^y = \text{Flow}(\mathbf{y}) . \quad (6)$$

Variable swapping for disentangling. We divide the latent space \mathcal{Z} into two sub-spaces, *i.e.*, clean image space and noise space, with separated latent codes $\mathbf{z} = [\mathbf{z}_c, \mathbf{z}_n]$. As shown in Figure 3(a), in order to ensure the noise information is decoupled from the noisy inputs, we introduce a noise variable swapping strategy to generate noisy image, *i.e.*, combining the noise variable \mathbf{z}_n^y from noisy input and the clean image variable \mathbf{z}_c^x from the clean counterpart as follows,

$$\hat{\mathbf{y}} = \text{Flow}^{-1}(\mathbf{z}_c^x, \mathbf{z}_n^y) \quad \hat{\mathbf{x}} = \text{Flow}^{-1}(\mathbf{z}_c^y, \mathbf{z}_n^x) , \quad (7)$$

where $\hat{\mathbf{y}}$ is the reconstructed noisy image, $\hat{\mathbf{x}}$ is the reconstructed clean image, and $\text{Flow}^{-1}(\cdot, \cdot)$ denotes the inverse process of $\text{Flow}(\cdot)$. Following Equation 7, we can easily derive the reconstructed noise $\hat{\mathbf{n}} = \hat{\mathbf{y}} - \hat{\mathbf{x}}$.

To ensure noise information is completely embedded in the noise variable \mathbf{z}_n , we impose a *reconstruction loss* to encourage recovery of the original noise \mathbf{n} and clean image \mathbf{x} , using the noise and clean image variables, respectively:

$$\mathcal{L}_{rec} = \|\hat{\mathbf{n}} - \mathbf{n}\|_1 + \|\hat{\mathbf{x}} - \mathbf{x}\|_1 . \quad (8)$$

Besides, to enforce the clean image code \mathbf{z}_c to contain only the noise-free content information, we employ a *content alignment loss* to align the structural features of noisy and clean image pairs, as

$$\mathcal{L}_{cnt} = \|\mathbf{z}_c^x - \mathbf{z}_c^y\|_1 . \quad (9)$$

Clean image regression. In addition, the denoised images can also be generated via its disentangled clean image component \mathbf{z}_c^y and a random variable \mathbf{z}_r as follow

$$\tilde{\mathbf{y}} = \text{Flow}^{-1}(\mathbf{z}_c^y, \mathbf{z}_r) . \quad (10)$$

We employ a *regression loss* on the generated $\tilde{\mathbf{y}}$ and further enforce the noise variable to be independent of the structure information, as

$$\mathcal{L}_{reg} = \|\tilde{\mathbf{y}} - \mathbf{x}\|_1 . \quad (11)$$

Besides, the restored image can be sampled by combing their internal clean image variable and a normal distribution variable in the testing stage as shown in Figure 3(b).

Noise correlation matrix. We assume that the additive noise \mathbf{n} is spatially uniform and uncorrelated (*e.g.*, *i.i.d.* Gaussian noise). Let $V : \mathbf{n} \mapsto V\mathbf{n} \in \mathbb{R}^{m \times M}$ be an overlapping patch extractor, where m denotes the number of pixels within one patch and M denotes the number of patches. We obtain the noise patch matrix $\hat{\mathbf{N}} = V\hat{\mathbf{n}} = [\hat{\mathbf{N}}_1, \hat{\mathbf{N}}_2, \dots, \hat{\mathbf{N}}_M]$ from the reconstructed $\hat{\mathbf{n}}$. The patch-wise noise correlation matrix is defined as

$$\Sigma = \frac{1}{M} \sum_{j=1}^M \hat{\mathbf{N}}_j \hat{\mathbf{N}}_j^T . \quad (12)$$

Based on the uncorrelated noise assumption, all of the non-diagonal elements of Σ should be as close to zero as possible. Denote the standard deviation of \mathbf{n} to be σ , the diagonal elements of Σ should all be σ^2 . Therefore, we set the following *noise correlation loss* as

$$\mathcal{L}_{noise} = \|\Sigma - \sigma^2 \mathbf{I}\|_F^2 . \quad (13)$$

Full objective function. By combining the above losses, the hybrid objective function \mathcal{L} used to train our model is

$$\mathcal{L} = \underbrace{\mathcal{L}_{reg}}_{\text{image}} + \underbrace{\alpha \mathcal{L}_{rec} + \beta \mathcal{L}_{cnt}}_{\text{disentangling}} + \underbrace{\gamma \mathcal{L}_{noise}}_{\text{noise}} , \quad (14)$$

Table 1: Quantitative results of denoised PSNR (in dB) \uparrow on CBSD68 (Roth and Black 2005), Kodak24 (Franzen 1999), and Set5 (Bevilacqua et al. 2012). The baseline methods include CBM3D (Dabov et al. 2007), CDnCNN (Zhang et al. 2017), and FFDNet (Zhang, Zuo, and Zhang 2018). In each column, the best result is highlighted in **bold**.

Datasets	estimated σ testing σ	$\sigma = 15$			$\sigma = 25$			$\sigma = 35$			$\sigma = 50$			$\sigma = 75$		
		10	15	20	20	25	30	30	35	40	45	50	55	70	75	80
CBSD68	CBM3D	34.68	33.52	29.51	31.27	30.71	28.69	29.33	28.89	27.54	27.53	27.38	26.93	25.87	25.74	25.45
	CDnCNN	34.68	33.89	29.06	31.68	31.23	28.50	29.81	29.58	27.63	28.05	27.92	26.83	24.35	24.47	24.44
	FFDNet	34.60	33.87	30.05	31.48	31.21	29.09	29.70	29.58	28.27	28.00	27.96	27.22	26.26	26.24	25.89
	FINO	34.96	34.05	30.81	31.82	31.43	29.52	29.96	29.76	28.45	28.24	28.21	27.34	26.49	26.45	26.08
Kodak24	CBM3D	35.33	34.28	30.21	32.32	31.68	29.68	30.53	29.90	28.52	28.81	28.46	28.12	27.16	26.82	26.66
	CDnCNN	35.23	34.48	29.21	32.28	32.03	28.93	30.57	30.46	28.26	28.98	28.85	27.76	25.00	25.04	24.69
	FFDNet	35.10	34.63	30.47	32.26	32.13	29.81	30.59	30.57	29.15	28.98	28.98	28.22	27.26	27.27	26.92
	FINO	35.41	34.67	30.68	32.57	32.31	30.10	29.21	30.62	29.31	29.35	29.14	28.45	27.65	27.54	27.33

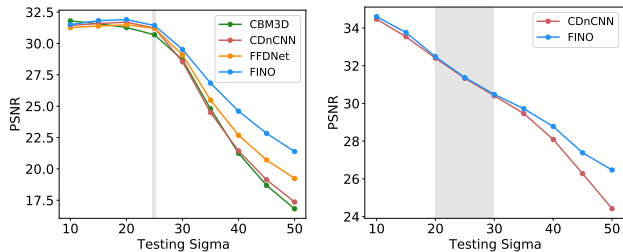


Figure 4: The generalization capability of the image denoising methods. All the methods are trained over a fixed ranges of noise levels which are indicated by the gray intervals.

where α , β , and γ are the weighting coefficients to balance the influence of each term.

Experiments

We evaluate the denoising performance of the proposed FINO on both synthetic and real noise with extensive experiments. FINO is implemented using PyTorch, which is tested on a GTX 2080Ti GPU. We adopt the ADAM optimizer with an initial learning rate of 4×10^{-4} . FINO employs two Flow Blocks and twelve coupling layers in each block. The ratio of clean image and noise variables is fixed as 3 : 1, since content contains richer texture and edge information. We set the hyper-parameters $\alpha = 1$, $\beta = 1$, and $\gamma = 0.1$. The network parameters are initialized randomly. During training, we randomly crop patches of resolution 144×144 from input images. We employ Peak Signal-to-Noise (PSNR) for the quantitative evaluation of denoised results. Since the real noisy degradation is relatively mild, causing small PSNR differences in some cases, we also report the Structural Similarity (SSIM) for real noise removal experiments.

Synthetic Noise Removal

We simulate spatially invariant additive white gaussian noise (AWGN) with different σ to evaluate the synthetic noise removal performance. We also evaluate if the denoising methods can be generalized to σ that is different from the training corpus. Besides the uniform noise, we further simulate spatially variant AWGN to evaluate the method’s robustness.

Spatially invariant AWGN. We evaluate the proposed method in AWGN removal on two widely-used image denoising datasets: CBSD68 (Roth and Black 2005) and Kodak24 (Franzen 1999). The CBSD68 dataset consists of 68 images from the separate testing set of the BSD300 dataset (Roth and Black 2005). The Kodak24 dataset consists of 24 center-cropped images of size 500×500 from the original Kodak dataset. We only use 200 images selected from the training set of the BSD dataset as training data. The noisy images are obtained by simulating AWGN of noise level $\sigma = 15, 25, 35, 50, 75$ to the clean counterpart. We compare the proposed FINO method with several state-of-the-art denoising methods, including one widely-used classic method (*i.e.*, CBM3D (Dabov et al. 2007)), and deep learning based methods (*i.e.*, CDnCNN (Zhang et al. 2017) and FFDNet (Zhang, Zuo, and Zhang 2018)). We first test FINO on noisy images corrupted by spatially invariant AWGN. In practice, it is difficult to estimate the noise level accurately, and the estimated noise level can vary in a range. Most existing methods are sensitive to the estimated noise level (Mohan et al. 2020), which means the performance would severely degrade while applied to wrongly estimated noise level. Hence, besides testing the performance when the estimated noise level is accurate, we also test the cases when the noise level is wrongly estimated. For model trained with each estimated σ , we test their performance on $\{\sigma - 5, \sigma, \sigma + 5\}$ truly sigma variance. The competing methods also are evaluated following the same settings. From the quantitative results shown in Table 1, our method outperforms all competing methods, especially for the wrong σ estimation cases. Although some competing methods are good at removing Gaussian noise when accurate noise estimation, their performance would be significantly degraded once the noise level is wrongly estimated, even slight variation as shown in Figure 4. The examples in Figure 5 also verify the observations in Table 1. With the merits of disentanglement and noise model, FINO has strong generalization capability comparing to other methods.

Spatially variant AWGN. We further evaluate the generalization capability of the proposed FINO to deal with spatially variant AWGN. We follow the spatially variant AWGN synthetic approach in (Zhang, Zuo, and Zhang 2018), which

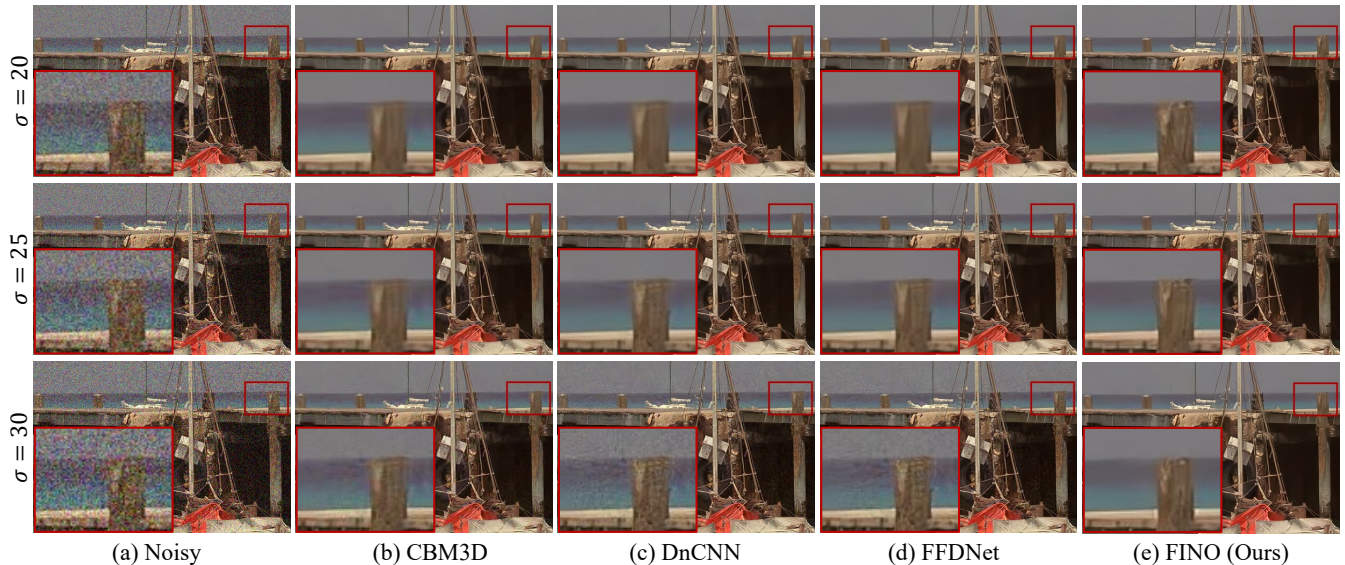


Figure 5: Examples of the denoised results on Kodak24 (Franzen 1999) dataset. From left to right, the input noisy image, the estimated results of CBM3D (Dabov et al. 2007), CDnCNN (Zhang et al. 2017), FFDNet (Zhang, Zuo, and Zhang 2018), and our method. All the methods are set/trained with the estimated noise level $\sigma = 25$. From top to down, the results for noisy images with $\sigma = 15$, $\sigma = 25$, and $\sigma = 35$.

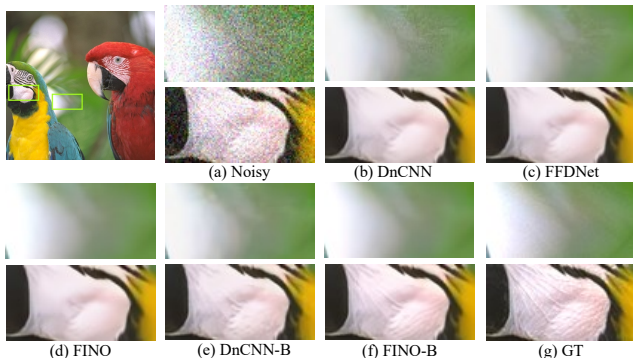


Figure 6: Generalization capacity of different methods on spatially variant noise removal ($\sigma \in (15, 35)$). All the methods are set/trained with the estimated noise level $\sigma = 25$, except to the blind denoising model, *i.e.*, CDnCNN-B and FINO-B.

generates a noise level map and applies it to images using element-wise multiplication. We select classic methods (CBM3D (Dabov et al. 2007)) and deep learning based methods (CDnCNN (Zhang et al. 2017), FFDNet (Zhang, Zuo, and Zhang 2018), and CDnCNN-B (blind version of CDnCNN) as the competing methods. In this experiment, we evaluate two versions of FINO: (1) FINO is trained on noisy images with specific $\sigma = 25$; (2) FINO-B is trained on noisy images with a σ range of $(0, 55]$. In the denoising stage, the ground truth noise level map is unavailable. All the methods are set/trained with the estimated noise level $\sigma = 25$, except to the CDnCNN-B, which is trained over a range of noise level $(0, 55]$ and does not need an estimated

Table 2: Quantitative results on the spatially variant noisy images on Kodak24 (Franzen 1999) dataset. All the methods are set/trained with the estimated uniform noise level $\sigma = 25$, while applying to spatially variant noisy images in the testing stage. Except to the blind denoising methods CDnCNN-B and FINO-B, since they need not estimated noise level.

Method	$\sigma \in (0, 50)$	$\sigma \in (15, 35)$
Noisy	20.66	20.58
CBM3D (Dabov et al. 2007)	29.66	31.16
CDnCNN (Zhang et al. 2017)	29.52	31.41
FFDNet (Zhang et al. 2017)	30.00	31.42
FINO (Ours)	31.15	32.01
CDnCNN-B (Zhang et al. 2017)	31.88	31.75
FINO-B (Ours)	32.43	32.36

noise level. The quantitative results are shown in Table 2. Our method outperforms all competing methods by large margins, and our blind denoising version also achieves better performances compared with CDnCNN-B. The examples shown in Figure 6 demonstrates our method can coarsely estimate the spatial noise level and effectively reconstruct the clean components, while the other competing methods deliver more over-smoothness or noisy residuum.

Real RGB Noise Removal

Finally, we evaluate the performance of different methods on a real-world dataset, which follows a more complicated noise distribution. In this experiment, we drop the noise modeling loss \mathcal{L}_{noise} , since the real noise in SIDD dataset

Table 3: Quantitative results on the real noisy SIDD dataset trained on SIDD medium dataset. The best result is in **bold**.

Method	PSNR \uparrow	SSIM \uparrow
DnCNN (Zhang et al. 2017)	23.66	0.583
TNRD (Chen and Pock 2016)	24.73	0.643
CBM3D (Dabov et al. 2007)	25.65	0.685
CBDNet(Guo et al. 2019)	33.28	0.868
GradNet (Liu et al. 2020)	38.34	0.953
AINDNet (Kim et al. 2020)	39.08	0.955
VDN (Yue et al. 2019)	39.26	0.955
InvDN (Liu et al. 2021)	39.28	0.955
FINO (Ours)	39.40	0.957

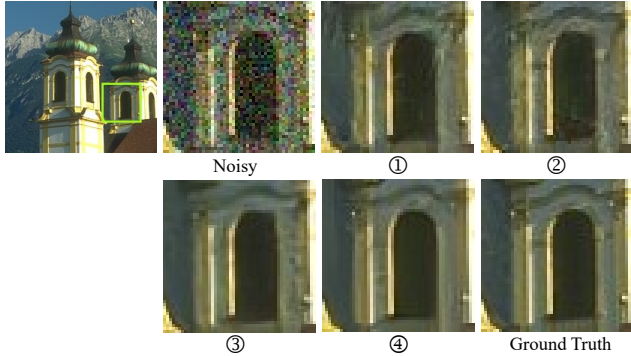


Figure 7: Visual examples of ablation study, including noisy image, results of four ablation experiments corresponding to the No. in Table 4, and ground truth.

seems against the uncorrelated noise assumption. Real noise stems from multiple sources, *e.g.*, short noise, thermal noise, and dark current noise, and is further affected by the in-camera processing (ISP) pipeline, which can be much more different from uncorrelated noise. We conduct real noise removal on the SIDD dataset (Abdelhamed, Lin, and Brown 2018), which is taken by five different types of smartphones. We utilize the medium SIDD dataset as the training set, which contains 320 clean and noise image pairs. We select classic denoising algorithm, CBM3D (Dabov et al. 2007), one blind Gaussian denoising method CDnCNN-B (Zhang et al. 2017), and real denoising methods, *i.e.*, CBDNet (Guo et al. 2019), GradNet (Liu et al. 2020), VDN (Yue et al. 2019), InvDN (Liu et al. 2021), as well as synthetic denoiser transferring to real noise, *i.e.*, AINDNet (Kim et al. 2020). The performance comparison on the test set of the SIDD dataset is listed in Table 3. The proposed FINO outperforms all competing methods. With the merits of the great generalization capability, the FINO can perform blind real image denoising without an external noise estimation module. Besides, the number of parameters of the FINO is (3.96M), which is much smaller than some competing methods, such as AINDNet (13.76M) and VDN (7.81M).

Ablation Study

Furthermore, we thoroughly investigate the impact of each loss function applied in the training stage. Table 4 shows

Table 4: Quantitative results of ablation study. Evaluated model is trained on $\sigma = 25$ and applied to $\sigma = 20, 25, 30$ for generalization capacity measurements. Note that all variant models include the regression loss \mathcal{L}_{reg} .

	\mathcal{L}_{cnt}	\mathcal{L}_{rec}	\mathcal{L}_{noise}	$\sigma = 25$		
				20	25	30
①		✓		31.67	31.20	29.17
②	✓			31.66	31.24	29.34
③	✓	✓		31.80	31.32	29.47
④	✓	✓	✓	31.82	31.43	29.52

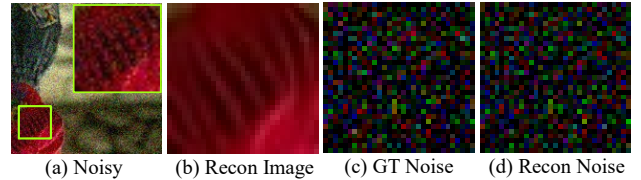


Figure 8: Visualization of reconstructed image and noise. We amplified the real noise (c) and reconstructed noise (d) with $2\times$ for better visibility.

the evaluation results and Figure 7 demonstrates the visual examples on different combination of loss functions. Visual quality of results by FINO without content alignment loss and reconstruction loss drop significantly as shown in the ① and ② in Figure 7. Without the content alignment loss, the generalization capability decreases largely, especially for the robustness for the higher noise as shown in the ① in Table 4. Without the reconstruction loss, the generalization capability would decrease since lacking a strong disentangling constraint. The visual example in Figure 7 also verifies the result with noise loss preserves more structural details.

Visualization of Noise Disentanglement

To better understand the noise model in FINO, we visualize the reconstructed noise and image outputs in Figure 8(b) and (c), respectively. We observe that the reconstructed noise is highly consistent with the ground truth one, demonstrating the effectiveness of FINO’s noise modeling.

Conclusion

In this work, we propose a Flow-based joint Image and Noise model (FINO) to tackle image denoising problems, which aim to estimate the underlying clean image from its noisy measurements. FINO distinctly decouples the image and noise components in the latent space and re-couples them via invertible transformations. Based on that, we employ joint image and noise modeling, *i.e.*, image priors can be learned from the noise-free training corpus, and the noise components are modeled based on the uncorrelated noise assumption. Our experimental results show promising results on both synthetic noise and real noise removal. Furthermore, we demonstrate that our method has superior generalization capability to the removal of non-uniform noise and noise with inaccurate estimation.

References

- Abdelhamed, A.; Brubaker, M. A.; and Brown, M. S. 2019. Noise flow: Noise modeling with conditional normalizing flows. In *Proceedings of the IEEE International Conference on Computer Vision (ICCV)*, 3165–3173.
- Abdelhamed, A.; Lin, S.; and Brown, M. S. 2018. A High-Quality Denoising Dataset for Smartphone Cameras. In *Proceedings of the IEEE Conference on Computer Vision and Pattern Recognition (CVPR)*.
- Anwar, S.; and Barnes, N. 2019. Real image denoising with feature attention. In *Proceedings of the IEEE International Conference on Computer Vision (ICCV)*, 3155–3164.
- Ardizzone, L.; Lüth, C.; Kruse, J.; Rother, C.; and Köthe, U. 2019. Guided image generation with conditional invertible neural networks. *arXiv preprint arXiv:1907.02392*.
- Bevilacqua, M.; Roumy, A.; Guillemot, C.; and line Alberi Morel, M. 2012. Low-Complexity Single-Image Super-Resolution based on Nonnegative Neighbor Embedding. In *Proceedings of the British Machine Vision Conference*, 135.1–135.10. BMVA Press. ISBN 1-901725-46-4.
- Chen, Y.; and Pock, T. 2016. Trainable nonlinear reaction diffusion: A flexible framework for fast and effective image restoration. *IEEE transactions on pattern analysis and machine intelligence*, 39(6): 1256–1272.
- Dabov, K.; Foi, A.; Katkovnik, V.; and Egiazarian, K. 2007. Color image denoising via sparse 3D collaborative filtering with grouping constraint in luminance-chrominance space. In *IEEE International Conference on Image Processing (ICIP)*, volume 1, 1–313. IEEE.
- Dinh, L.; Krueger, D.; and Bengio, Y. 2014. Nice: Non-linear independent components estimation. *arXiv preprint arXiv:1410.8516*.
- Dinh, L.; Sohl-Dickstein, J.; and Bengio, S. 2016. Density estimation using real nvp. *arXiv preprint arXiv:1605.08803*.
- Elad, M.; and Aharon, M. 2006. Image Denoising Via Sparse and Redundant Representations Over Learned Dictionaries. *IEEE Transactions on Image Processing*, 15(12): 3736–3745.
- Franzen, R. 1999. Kodak lossless true color image suite. source: <http://r0k.us/graphics/kodak>, 4(2).
- Gu, S.; Zhang, L.; Zuo, W.; and Feng, X. 2014. Weighted nuclear norm minimization with application to image denoising. In *Proceedings of the IEEE Conference on Computer Vision and Pattern Recognition (CVPR)*, 2862–2869.
- Guo, S.; Yan, Z.; Zhang, K.; Zuo, W.; and Zhang, L. 2019. Toward convolutional blind denoising of real photographs. In *Proceedings of the IEEE Conference on Computer Vision and Pattern Recognition (CVPR)*, 1712–1722.
- Ho, J.; Chen, X.; Srinivas, A.; Duan, Y.; and Abbeel, P. 2019. Flow++: Improving flow-based generative models with variational dequantization and architecture design. In *International Conference on Machine Learning*, 2722–2730. PMLR.
- Kim, Y.; Soh, J. W.; Park, G. Y.; and Cho, N. I. 2020. Transfer learning from synthetic to real-noise denoising with adaptive instance normalization. In *Proceedings of the IEEE Conference on Computer Vision and Pattern Recognition (CVPR)*, 3482–3492.
- Kingma, D. P.; and Dhariwal, P. 2018. Glow: Generative Flow with Invertible 1x1 Convolutions. In Bengio, S.; Wallach, H.; Larochelle, H.; Grauman, K.; Cesa-Bianchi, N.; and Garnett, R., eds., *Advances in Neural Information Processing Systems (NeurIPS)*, volume 31. Curran Associates, Inc.
- Kingsbury, N.; and Magarey, J. 1998. Wavelet transforms in image processing. In *Signal analysis and prediction*, 27–46. Springer.
- Kirichenko, P.; Izmailov, P.; and Wilson, A. 2020. Why normalizing flows fail to detect out-of-distribution data. *Advances in Neural Information Processing Systems (NeurIPS)*, 2020-December.
- Liu, D.; Wen, B.; Fan, Y.; Loy, C. C.; and Huang, T. S. 2018. Non-local recurrent network for image restoration. In *Advances in Neural Information Processing Systems (NeurIPS)*, 1673–1682.
- Liu, Y.; Anwar, S.; Zheng, L.; and Tian, Q. 2020. Gradnet image denoising. In *Proceedings of the IEEE Conference on Computer Vision and Pattern Recognition (CVPR)*, 508–509.
- Liu, Y.; Qin, Z.; Anwar, S.; Ji, P.; Kim, D.; Caldwell, S.; and Gedeon, T. 2021. Invertible Denoising Network: A Light Solution for Real Noise Removal. In *Proceedings of the IEEE Conference on Computer Vision and Pattern Recognition (CVPR)*, 13365–13374.
- Lugmayr, A.; Danelljan, M.; Van Gool, L.; and Timofte, R. 2020. Srfflow: Learning the super-resolution space with normalizing flow. In *Proceedings of the European Conference on Computer Vision (ECCV)*, 715–732. Springer.
- Mohan, S.; Kadkhodaie, Z.; Simoncelli, E. P.; and Fernandez-Granda, C. 2020. Robust And Interpretable Blind Image Denoising Via Bias-Free Convolutional Neural Networks. In *International Conference on Learning Representations*.
- Plötz, T.; and Roth, S. 2018. Neural Nearest Neighbors Networks. In *Advances in Neural Information Processing Systems (NeurIPS)*.
- Ravishanker, S.; and Bresler, Y. 2012. Learning sparsifying transforms. *IEEE Transactions on Signal Processing*, 61(5): 1072–1086.
- Roth, S.; and Black, M. J. 2005. Fields of experts: A framework for learning image priors. In *Proceedings of the IEEE Conference on Computer Vision and Pattern Recognition (CVPR)*, volume 2, 860–867. IEEE.
- Xiao, M.; Zheng, S.; Liu, C.; Wang, Y.; He, D.; Ke, G.; Bian, J.; Lin, Z.; and Liu, T.-Y. 2020. Invertible image rescaling. In *Proceedings of the European Conference on Computer Vision (ECCV)*, 126–144. Springer.
- Xu, J.; Zhang, L.; Zuo, W.; Zhang, D.; and Feng, X. 2015. Patch group based nonlocal self-similarity prior learning for image denoising. In *Proceedings of the IEEE International Conference on Computer Vision (ICCV)*, 244–252.

Yue, Z.; Yong, H.; Zhao, Q.; Zhang, L.; and Meng, D. 2019. Variational denoising network: Toward blind noise modeling and removal. *arXiv preprint arXiv:1908.11314*.

Zhang, K.; Zuo, W.; Chen, Y.; Meng, D.; and Zhang, L. 2017. Beyond a gaussian denoiser: Residual learning of deep cnn for image denoising. *IEEE Transactions on Image Processing*, 26(7): 3142–3155.

Zhang, K.; Zuo, W.; and Zhang, L. 2018. FFDNet: Toward a fast and flexible solution for CNN-based image denoising. *IEEE Transactions on Image Processing*, 27(9): 4608–4622.